Integral invariants and decay of temporally developing grid turbulence

T. Watanabe, and K. Nagata

Citation: Physics of Fluids **30**, 105111 (2018); doi: 10.1063/1.5045589
View online: https://doi.org/10.1063/1.5045589
View Table of Contents: http://aip.scitation.org/toc/phf/30/10
Published by the American Institute of Physics

Integral invariants and decay of temporally developing grid turbulence

T. Watanabe[a] and K. Nagata[b]
Department of Aerospace Engineering, Nagoya University, Nagoya 464-8603, Japan

(Received 21 June 2018; accepted 11 October 2018; published online 31 October 2018)

We present a study of a large-scale energy spectrum and integral invariants in temporally developing grid turbulence at mesh Reynolds numbers of $Re_M = 10\,000$ and $20\,000$ by employing direct numerical simulations (DNSs) in a periodic box. The simulations are initialized with a velocity field that approximates the wakes induced by the bars of conventional square grids. The turbulence statistics obtained in the temporal DNS agree well with those of the previous experiments in both the production and decay regions. The temporally developing grid turbulence also has a so-called non-equilibrium region, which is consistent with its spatially developing counterpart, where the normalized dissipation rate of turbulence kinetic energy (TKE), C_ε, increases as the turbulence decays. The decay exponent n of TKE is $n = 1.22$ at $Re_M = 20\,000$ and $n = 1.35$ at $Re_M = 10\,000$, which are close to the values for the Saffman turbulence [i.e., 6/5 for $Re_M = 20\,000$ and $6(1 + p)/5 \approx 1.36$ for $Re_M = 10\,000$ with $p \approx 0.13$ obtained by $C_\varepsilon \sim t^p$ at large t]. The longitudinal integral length scale and the TKE dissipation rate also exhibit temporal evolutions consistent with the Saffman turbulence for both Re_M. The Saffman integral directly evaluated in the grid turbulence tends to be time-independent after the turbulence evolves for about 200 times of characteristic time scale defined by mesh size divided by the mean velocity of a fluid passing the grid. A direct evaluation of the TKE spectrum $E(k)$ shows that $E(k) \approx Lk^2/4\pi^2$ is valid for a finite range of low wavenumbers. *Published by AIP Publishing.*
https://doi.org/10.1063/1.5045589

I. INTRODUCTION

Turbulence appears in various scientific problems related to fluid mechanics. One of the simplest turbulent flows is homogeneous isotropic turbulence, for which the statistical descriptions of three-dimensional turbulent flows are simplified and a large number of turbulence theories and models have been developed before. Without an external force that sustains turbulence, turbulent kinetic energy (TKE) in homogeneous isotropic turbulence decays with time. The decay rate of the TKE in homogeneous isotropic turbulence has been studied extensively with theoretical, experimental, and numerical approaches because of the importance of TKE in practical problems, such as the mixing process in chemical engineering,[1] combustion in internal combustion engines,[2] and environmental flows,[3,4] where the TKE and its dissipation rate play important roles for predicting these flows. The decay exponent n of TKE in freely decaying, homogeneous isotropic turbulence is related to the form of the energy spectrum at low wavenumbers.[5,6] The TKE spectrum $E(k)$ at low wavenumbers can be written from the Taylor series expansion as[6]

$$E(k) = \frac{Lk^2}{4\pi^2} + \frac{Ik^4}{24\pi^2} + \cdots, \tag{1}$$

where k is the wavenumber, and L and I are the Saffman and Loitsyansky integrals, respectively, which are defined as follows:

$$L = \int \langle \mathbf{u}(\mathbf{x}) \cdot \mathbf{u}(\mathbf{x} + \mathbf{r}) \rangle d\mathbf{r}, \tag{2}$$

$$I = -\int \mathbf{r}^2 \langle \mathbf{u}(\mathbf{x}) \cdot \mathbf{u}(\mathbf{x} + \mathbf{r}) \rangle d\mathbf{r}, \tag{3}$$

where $\mathbf{u}(\mathbf{x})$ is the velocity fluctuation vector, $\mathbf{r}$ represents the separation vector, and the bracket denotes averaging, which is usually computed with spatial average in homogeneous isotropic turbulence. The Saffman and Loitsyansky integrals can be related to the linear momentum and the angular momentum, respectively.[6] In a Saffman turbulence,[7] $E(k)$ at low wavenumbers is given by $E(k) = Lk^2/4\pi^2$. In this case, the TKE decays with time t according to $\langle u^2 \rangle \sim t^{-6/5}$. By contrast, in a Batchelor turbulence,[5,8] where $L \approx 0$, $E(k)$ at low wavenumbers is given by $E(k) = Ik^4/24\pi^2$. In this case, TKE decays according to Kolmogorov's decay law[9] $\langle u^2 \rangle \sim t^{-10/7}$. In the present paper, the symbol $\sim$ means "varies as" or "scales with," following the definition used in Ref. 10. On the other hand, the symbol $\approx$ is used when two quantities are approximately equal to each other.

Grid turbulence has been studied in laboratory experiments for verifying the theories developed for freely decaying, homogeneous isotropic turbulence.[11,12] Even though these studies have invented various methods to produce grid turbulence which is close to freely decaying, homogeneous isotropic turbulence, grid turbulence reported even in recent studies is still different from ideal freely decaying, homogeneous isotropic turbulence. For example, many studies have reported that the root-mean-square (rms) velocity fluctuation in the streamwise direction is slightly higher than those in the transverse directions.[12–19] The theoretical treatment of the infinitely small wavenumber $k \to 0$ also causes difficulty in interpreting the results from experiments and numerical simulations since the flow in the wavenumber space at

[a]watanabe.tomoaki@c.nagoya-u.jp
[b]nagata@nagoya-u.jp

$k \to 0$ is always affected by the boundaries even if the boundaries in physical space are very far from the region of interest so that the decay of grid turbulence does not seem to be influenced by the boundaries. Grid turbulence can be, at the best, an approximation of freely decaying, homogeneous isotropic turbulence. However, it has been studied in relation to the theories of freely decaying, homogeneous isotropic turbulence.[18,20,21]

It has been widely accepted that TKE follows the power law in the decay region far from the grid[18,22,23] (typically $x \geq 40$–$50M$),

$$TKE \sim \frac{3}{2}\frac{\langle u^2 \rangle}{U_0^2} = A\left(\frac{x}{M} - \frac{x_0}{M}\right)^{-n}, \tag{4}$$

where M is the mesh size, x is the streamwise distance from the grid, x_0 is the virtual origin, U_0 is the mean wind speed, A is the decay constant, and n is the decay exponent.

An extensive review of the decay exponent in grid turbulence was performed in our previous paper.[18] Krogstad and Davidson[20] showed that $n = 1.13 \pm 0.02$ and $\langle u^2 \rangle L_u^3$ is constant during decay, which is required for the invariance of the Saffman integral. Here, L_u $(= \int_0^\infty f(r)dr$, where $f(r) = \langle u(x, y, z)u(x + r, y, z)\rangle / \langle u(x)^2 \rangle)$ is the longitudinal integral length scale of u. Kitamura *et al.*[18] also showed that $\langle u^2 \rangle L_u^3$ is constant during decay for the examined mesh Reynolds number $Re_M = U_0 M/\nu$ range of 6700–33 000 (ν is the kinematic viscosity), regardless of the grid geometry (i.e., square bar or round bar). Sinhuber *et al.*[21] conducted experiments on a high-Reynolds-number grid turbulence ($10^4 < Re_M < 5 \times 10^6$) and found that $n = 1.18 \pm 0.02$, which is close to Saffman's prediction of 6/5 and independent of Re_M. Djenidi, Kamruzzaman, and Antonia[23] argued that most reported data fall in the transition period (i.e., $10^0 < Re_\lambda < 10^2$), where n increases towards the value in the final period of decay. This implies that one cannot determine solely on the basis of the value of n whether the grid turbulence is close to a Saffman or a Batchelor turbulence and whether it follows the Saffman or Kolmogorov decay laws at low Re_λ ($<10^2$).

These recent experiments have found that the grid turbulence follows the Saffman decay law. However, the grid turbulence that follows the Kolmogorov decay law in the final period of decay was also reported in the wind tunnel experiments.[24] These studies indicate that the grid turbulence is mostly the Saffman turbulence, but it can be the Batchelor turbulence on some occasions. Recent experiments that confirmed the Saffman decay law in grid turbulence did not answer why their grid turbulence behaves like the Saffman turbulence. The answer must be related to the production process of turbulence rather than the decay exponent of the TKE because the decay exponent should be determined by how turbulence is generated before it begins to decay. Most studies of grid turbulence focus on its decay, and they have not investigated how the nature of Saffman or Batchelor turbulence prevails during the production phase of grid turbulence. It is important to stress that the flow is not turbulent in the region very close to the grid, and neither the Saffman nor the Batchelor turbulence exists before turbulence is well developed in the production region. Therefore, a more straightforward method of investigating this issue may be a direct evaluation of $E(k)$ at low wavenumbers and Saffman and Loitsyansky integrals (i.e., L and I, respectively) in grid turbulence in both production and decay regions. However, direct evaluations have not been done in grid turbulence because of the difficulty in obtaining $E(k)$ at small k or calculating L and I through experiments or a direct numerical simulation (DNS) of a spatially developing (decaying) grid turbulence.[25–29]

Temporal simulations have been performed for turbulent shear flows, such as jets,[30,31] wakes,[32,33] mixing layers,[34,35] and boundary layers,[37] and have proven to be very effective for studying various canonical flows. These temporal simulations use periodic boundary conditions in the streamwise direction even if all these flows are inhomogeneous in this direction. Thus, the statistics in the temporal simulations vary with time rather than in the streamwise direction. Even though temporally developing turbulent shear flows are homogeneous in the streamwise direction unlike the spatially developing counterparts, temporal simulations have successfully reproduced the important characteristics of these flows, e.g., cross-streamwise profiles of various statistics,[30,37] mean momentum transport,[37] and mass entrainment rate.[38] Differences between spatially and temporally developing turbulent shear flows are also well known. For example, homogeneity in the streamwise direction results in the different form of the averaged continuity equation, from which we can show that the mean cross-streamwise velocity is zero in temporally developing planar jets although the spatial jet induces the inward velocity outside the jet. Despite the success of the temporal simulations of canonical flows, grid turbulence has not been considered in this manner. This study considers the temporally developing grid turbulence, which is a counterpart to the spatially developing grid turbulence, in a similar spirit to the temporal counterparts studied for the canonical flows. The bars of the grid produce the wakes behind them, and the wakes merge to form the grid turbulence. Therefore, the present DNS resembles the temporal simulations of turbulent wakes.[33] The temporal DNS has a great advantage against the spatial DNS in terms of computational cost, which enables us to simulate the grid turbulence with a fine spatial resolution for resolving the smallest scale in a very large computational domain with respect to the integral scale.

We perform a DNS of the grid turbulence in a periodic box based on the temporal approach and directly calculate the three-dimensional energy spectrum $E(k)$, Saffman integral L, and decay exponent n. This approach allows us to investigate the direct link between the energy spectrum at low wavenumbers and the decay exponent n in the grid turbulence, which is more straightforward than calculating related (indirect) statistics, such as $\langle u^2 \rangle L_u^{m+1}$, where $E(k) \sim C_m k^m$ for small k (C_m being the invariant for $m \leq 4$ in exact homogeneous isotropic turbulence).[20] The simulations are initialized with the velocity field that approximates the flow induced by the conventional square grids towed at a constant speed. This temporally developing (decaying) simulation has several notable advantages compared with the spatially developing (decaying) DNS in terms of the points that follow. First, the temporally developing (decaying) simulation can be done in a periodic box and does not require an extremely long computational domain in the streamwise direction. Note again that a freely decaying

turbulence can be achieved in a wind tunnel beyond 40–50M from the grid[18,23] to ensure a satisfactory homogeneity. This allows us to expand the domain in transverse directions for fixed computer resources, which is very important for investigating large-scale characteristics. Second, the temporal simulation does not need to resolve the grid surface, where setting proper boundary conditions and ensuring numerical accuracy are generally difficult for small bars.[13,39] Note that one should set up a small mesh size M if one wants to ensure a large computational domain compared with the characteristic eddy size (e.g., L_u) for a fixed streamwise extent of the computational domain. Therefore, small grid bars to ensure that the solidity of the grid falls within the range $\sigma = 0.34$–0.44 are used in most grid turbulence experiments.[12] We first show that the overall features of the grid turbulence in the temporal simulations, including derivative quantities, agree well with the existing experiments of grid turbulence. We then discuss the three-dimensional energy spectrum and Saffman integral.

So far, there is no consensus about the conditions under which the grid turbulence behaves as the Saffman turbulence or Batchelor turbulence. Comparisons among different experimental setups are encouraged to settle this problem (e.g., comparison between the towed grid and static grid, active and passive grids, and cylindrical and rectangular rods). The temporal grid turbulence simulated here is not exactly the same as the grid turbulence studied in the experiments using a static grid. However, we find that the temporal grid turbulence possesses various characteristics that have been found in grid turbulence experiments. To the best of the authors' knowledge, this is the first direct evaluation of $E(k)$ and integral invariants in a grid turbulence.

One of the important questions is, why the Saffman or Batchelor turbulence prevails in grid turbulence? This is what the existing theories for decaying homogeneous isotropic turbulence cannot answer because the shape of the energy spectrum is presumed as a starting point of the theory. A very large-scale field is also produced as the grid turbulence develops from a laminar state, and the DNS of the temporally developing grid turbulence enables us to observe this production process in the wavenumber space. Large scale structures are known to be flow dependent. Therefore, the decay law found for grid turbulence might not be universal because the decay of turbulence is expected to depend on large scales of turbulence. However, it is interesting to investigate the decay of grid turbulence in relation to the turbulent kinetic energy spectrum at a low wavenumber. This study is also practically important for the modeling of $E(k)$ at large scales.[40] The models for $E(k)$ can be used as an initial condition in simulations, such as DNS in a periodic box and spectral closures like eddy-damped quasi-normal Markovian model,[41,42] and an inflow velocity disturbance for simulations of inhomogeneous turbulent flows.[43]

II. DNS OF A TEMPORALLY DEVELOPING GRID TURBULENCE

The flow considered is a grid turbulence generated by a square grid with a mesh size M towed with speed U_0 (Fig. 1). The DNS for the temporally developing grid turbulence is performed using the methodology applied for temporally developing free shear flows. The governing equations are incompressible Navier–Stokes equations

$$\frac{\partial U_i}{\partial x_i} = 0, \tag{5}$$

$$\frac{\partial U_i}{\partial t} + \frac{\partial U_i U_j}{\partial x_j} = -\frac{\partial P}{\partial x_i} + \nu \frac{\partial^2 U_i}{\partial x_j \partial x_j}, \tag{6}$$

where U_i is the ith component of the velocity vector and P is the pressure divided by a constant fluid density. The thickness of each bar consisting of the grid is $d = 0.2M$, yielding $\sigma = 0.36$. The Reynolds number based on the bar thickness, $Re_d = U_0 d/\nu$, is defined along with Re_M. The Reynolds numbers are $Re_M = 10\,000$ ($Re_d = 2000$) and $20\,000$ (4000). The DNS is performed excluding the turbulence grid in the computational domain, following the temporal simulations of the turbulent wakes with periodic boundary conditions in the streamwise direction.[32,33,44–46] We considered a cubic computational domain with a side length l, where periodic boundary conditions are applied in three directions. The computational domain is represented by N^3 grid points. Table I summarizes the parameters in the DNS. The DNS at $Re_M = 10\,000$ is performed with $l = 20M$ (Re1a) and $30M$ (Re1b) to examine the influences of the domain size while $l = 10M$ is used for $Re_M = 20\,000$.

The simulations of the temporally developing grid turbulence are initialized as follows:

$$U = \langle U \rangle_x + u', V = v', W = w', \tag{7}$$

where U, V, and W are the instantaneous velocity in x, y, and z directions, respectively, whilst u', v', and w' are the fluctuating components. $\langle \cdot \rangle_x$ denotes the average taken in the x direction represented as a function of y and z. The initial mean velocity profile is homogeneous in the x direction and given as a

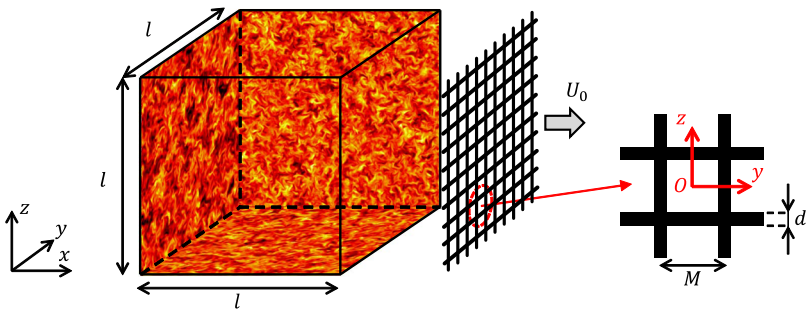

FIG. 1. DNS of the grid turbulence generated by a grid towed with speed U_0. The statistics are computed in the coordinate whose origin is located at the center of the grid.

TABLE I. Parameters in the DNS. The DNS is performed until $t = T_{end}$.

Run	Re_M	l	N^3	δ/M	δ/d	T_{end}
Re1a	10 000	$20M$	2304^3	0.0087	0.043	$1024M/U_0$
Re1b	10 000	$30M$	3456^3	0.0087	0.043	$256M/U_0$
Re2	20 000	$10M$	2048^3	0.0049	0.024	$1024M/U_0$

function of (y, z)

$$\langle U\rangle_x = \begin{cases} U_0 \text{ (behind grid bars)} \\ 0 \quad \text{(in other locations)} \end{cases}. \tag{8}$$

The flow induced by the towed grid is modeled with the top-hat profile by Eqs. (7) and (8). The numerical simulations of spatially developing wakes also produced a similar top-hat-like velocity profile behind a cylinder[47,48] with Re_d close to the present DNS. The velocity fluctuations generated by a diffusion process[49] are used in Eq. (7) for the turbulent wake development of the bars, where the rms velocity is 0.5% of U_0 and the characteristic length scale of the fluctuations is $0.2M$. The velocity fluctuations correspond to the background turbulence observed in wind tunnel experiments. A similar level of the background turbulence intensity was indeed reported.[18,50] As is the case in almost all the grid turbulence experiments, the background velocity fluctuations are much weaker than the turbulence produced by the grid. The initial velocity profile is corrected such that it satisfies $\nabla\cdot\mathbf{U} = 0$ by solving the Poisson equation for pressure. With this initialization, the turbulent wakes of the bars develop with time from a laminar state and merge to form the grid turbulence.

The temporally developing grid turbulence is produced from a transverse profile of the mean streamwise velocity that approximates the flow past a grid. This approximation is good only for the mean streamwise velocity and is much simpler than the flow in grid turbulence in the wind tunnel since the approximation ignores other possible influences of grid geometry. An implicit assumption in the temporal simulation of towed grid turbulence is that U_0 is large enough for statistics to be approximately homogeneous in the x direction even at an early time. Therefore, the difference might exist in the process of formation of grid turbulence that occurs near the grid because the temporal simulation cannot include the grid object.

The time is advanced from the initial field with the DNS code based on the fractional step method after the flow is initialized by Eqs. (7) and (8). The spatial derivative is computed by a fourth-order fully conservative finite difference,[51] whilst time is advanced using the third-order Runge–Kutta method, in which the time step is set by a constant Courant number of 0.6. The Poisson equation is solved using the biconjugate gradient stabilized (Bi-CGSTAB) method.[52] The DNS code is used in our previous studies with different boundary and initial conditions.[53,54] The simulation is advanced until $t = 1024t_r$ for Re1a and Re2 and until $t = 256t_r$ for Re1b, where $t_r = M/U_0$. Meanwhile, the flow is statistically homogeneous in the x direction. Therefore, the average in the x direction, $\langle\cdot\rangle_x$, is taken in each snapshot as a function of (y, z) with the origin at the grid center as in Fig. 1. The statistics are calculated for the region of $-0.5M \le y, z \le 0.5M$ because the turbulence grid is made with repetitions of the square shape. The temporally developing grid turbulence is always statistically homogeneous in the x direction. Furthermore, the homogeneity in the y and z directions is achieved once the grid turbulence has developed. Therefore, we also use volume average in the entire computational domain, which is denoted by $\langle\cdot\rangle$. Hereafter, $\mathbf{u}$ denotes a fluctuating velocity vector from the volume averaged velocity $\mathbf{u} = \mathbf{U} - \langle\mathbf{U}\rangle$.

The length $X = tU_0$ in the temporally developing grid turbulence is equivalent to a streamwise distance x from the grid in the spatially developing grid turbulence in wind tunnel experiments. Then, the nondimensional time $t/t_r = X/M$, where $t_r = M/U_0$ is equivalent to the nondimensional streamwise distance x/M in wind tunnel experiments. Therefore, the temporally developing grid turbulence is compared with the spatially developing grid turbulence by plotting the results against X/M or t/t_r.

Figure 2(a) shows the temporal evolutions of the computational grid size δ relative to the Kolmogorov scale $\eta = (\nu^3/\varepsilon)^{1/4}$, where $\varepsilon = 2\nu\langle S_{ij}S_{ij}\rangle_x$ is the kinetic energy dissipation rate [$S_{ij} = (\partial U_i/\partial x_j + \partial U_j/\partial x_i)/2$: total strain tensor]. $\delta \approx 2\eta$ for the minimum value of η in the simulations. η increases with time; hence, δ is smaller than η for most of the decay period of grid turbulence. The central difference scheme used in the DNS was shown to well capture the spectrum of the kinetic energy dissipation rate at small scales at $\delta/\eta \approx 2.3$ in Ref. 55.

Figure 2(b) presents the size of the computational domain divided by $L_u = \int_0^\infty f(r)dr$, where the integral is terminated at the first separation distance r at which $f(r)$ reaches 0. A computational domain should be much larger than the integral length scale such that the periodicity imposed by the boundary conditions has negligible influences on the flow

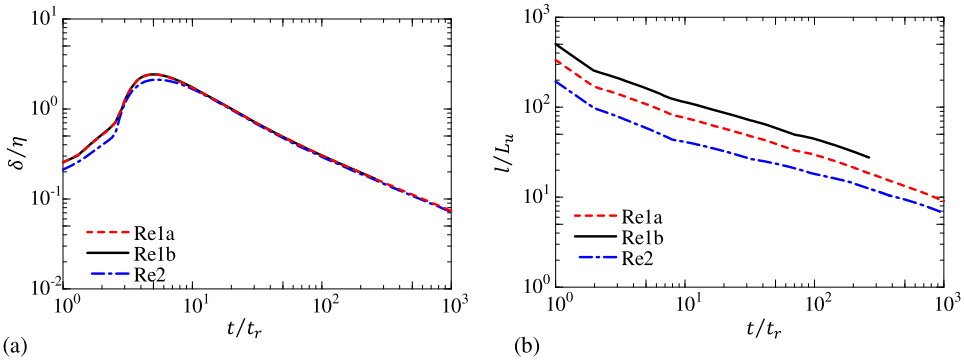

FIG. 2. Temporal evolutions of (a) spatial resolution and (b) computational domain size relative to the Kolmogorov scale η and the integral length scale L_u, respectively. η is calculated with $\varepsilon = 2\nu\langle S_{ij}S_{ij}\rangle_x$ at $(y, z) = (0, 0)$.

evolution.[6] Note that the present DNS uses a larger computational domain l/M than that in the previous grid turbulence simulations.[25–29,60]

III. RESULTS AND DISCUSSIONS

A. Development of grid turbulence

Figure 3 shows the instantaneous streamwise velocity U on the surface of the computational box from $t/t_r = 0$ to 24. The imprint of the initial mean velocity profile clearly remains at an early time. The shear that results from the mean velocity causes the turbulent wakes of the bars to grow with time, as shown in Figs. 3(b) and 3(c). The turbulent wakes produced by the bar merge to form the grid turbulence in Figs. 3(d) and 3(e). The grid turbulence approaches a homogeneous isotropic turbulence at later times in Fig. 3(f). The vortical structures at $t/t_r = 24$ are visualized in Fig. 4 with the second invariant of the velocity gradient tensor $Q = (\omega_i\omega_i - 2S_{ij}S_{ij})/4$ (ω_i: vorticity). The region with the vorticity dominant over the strain is related to a positive Q, whilst the negative values of Q appear in the strain-dominant region, such as the proximity of the intense

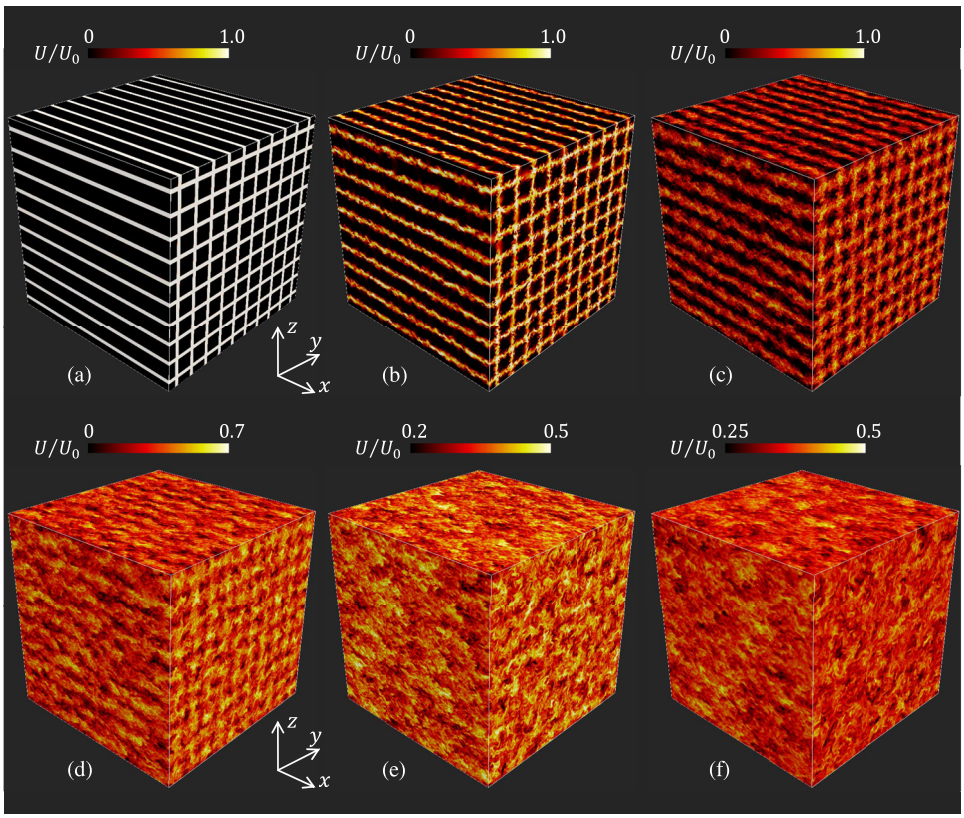

FIG. 3. Temporally developing grid turbulence in a periodic box. Instantaneous streamwise velocity U is visualized on the boundaries of the computational box. The results are taken at (a) $t/t_r = 0$, (b) $t/t_r = 2$, (c) $t/t_r = 4$, (d) $t/t_r = 8$, (e) $t/t_r = 16$, and (f) $t/t_r = 24$ from the DNS for $Re_M = 20\,000$.

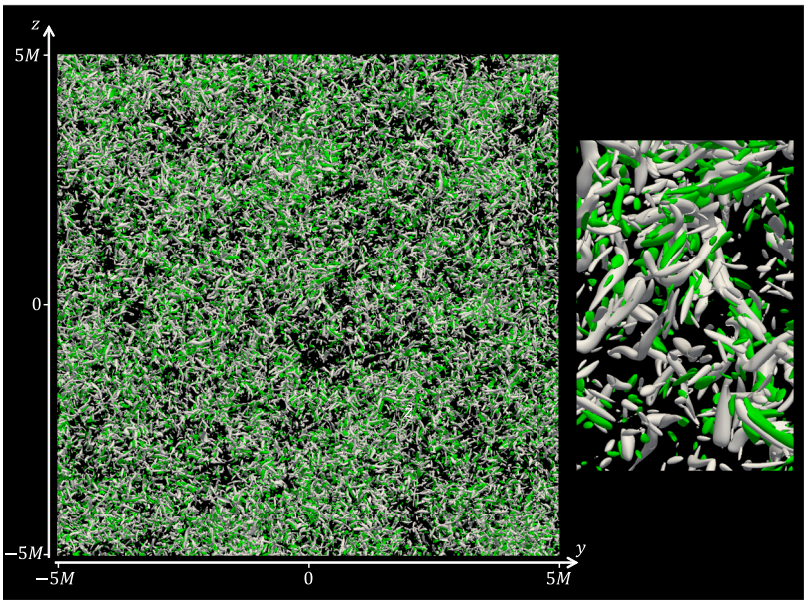

FIG. 4. Visualization of small scale vortical structures at $Re_M = 10\,000$ at $t/t_r = 24$ (Re1a). The isosurface of $Q/(1/t_r^2) = 1$ and $Q/(1/t_r^2) = -1$ is shown in white and green, respectively. The figure shows a part of the computational domain with side lengths of $4.2M$, $10M$, and $10M$ in the x, y, and z directions, respectively. The center region is magnified in the right figure.

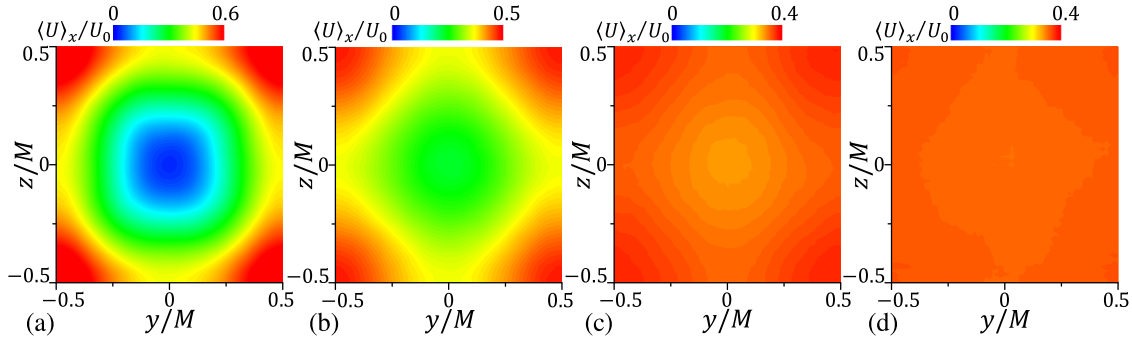

FIG. 5. Mean velocity profile at $Re_M = 20\,000$ at (a) $t/t_r = 4$, (b) $t/t_r = 8$, (c) $t/t_r = 16$, and (d) $t/t_r = 24$.

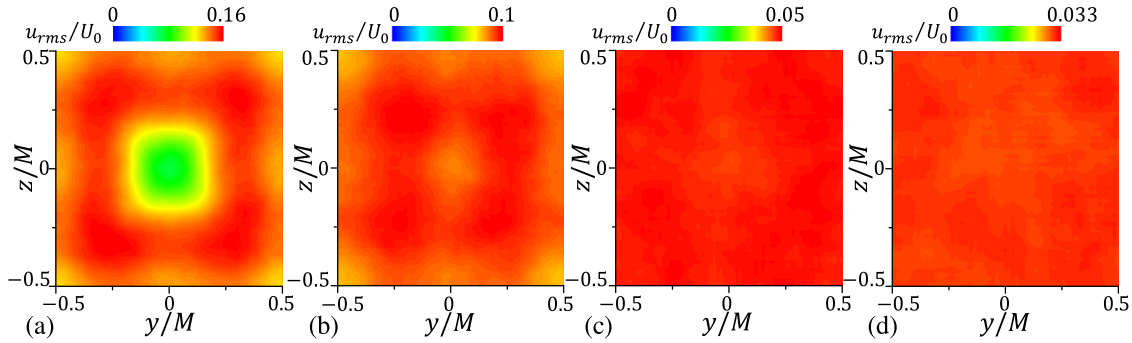

FIG. 6. Streamwise rms velocity at $Re_M = 20\,000$ at (a) $t/t_r = 4$, (b) $t/t_r = 8$, (c) $t/t_r = 16$, and (d) $t/t_r = 24$.

vortex.[6] At this time, the computational domain is filled with small-scale structures similar to the grid turbulence studied with the spatial DNS.[13,27,29]

Figures 5 and 6 present the mean velocity $\langle U\rangle_x$ and the rms velocity $u_{rms} = \langle u'^2\rangle_x^{1/2}$ on a y–z plane. The statistics are highly inhomogeneous at the initial stage of the DNS because of the inhomogeneous initial mean velocity profile. The spatial dependences of $\langle U\rangle_x$ and u_{rms} become small as turbulence grows with time, and the flow approaches the statistically homogeneous state. Figure 7 shows the temporal evolutions of $\langle U\rangle_x$ and u_{rms} at three locations of (y, z). The mean velocity becomes homogeneous at $t/t_r \approx 25$ and maintains a constant value $\langle U\rangle_x/U_0 = 0.36$ for the large t. This value is related to σ. Similarly, the rms velocity profile becomes independent of (y, z) with time. Figures 7(b) and 7(c) confirm that the flow maintains a statistically homogeneous state during the simulations once a y–z dependence of the rms velocity disappears. These temporal evolutions of the grid turbulence are similar for both $Re_M = 10\,000$ and 20 000.

B. Statistical properties: Comparison with experiments

The statistics in the temporally developing grid turbulence are compared with those in the experiments. Figures 7(b) and 7(c) also include the experimental results of the grid turbulence. Here, the DNS results are compared with the experimental results of Melina *et al.*[56] and Nagata *et al.*[57] because these papers present the statistics even for very small x/M. The experimental results of towed grid turbulence[59,61] are also shown in Fig. 7(c) because towed grid turbulence also decay with time. The temporally developing grid turbulence in the present DNS decays similarly to the spatially developing grid turbulence in the experiments in both the near-field [Fig. 7(b)] and decay regions [Fig. 7(c)]. Note that the rms velocity measured in the

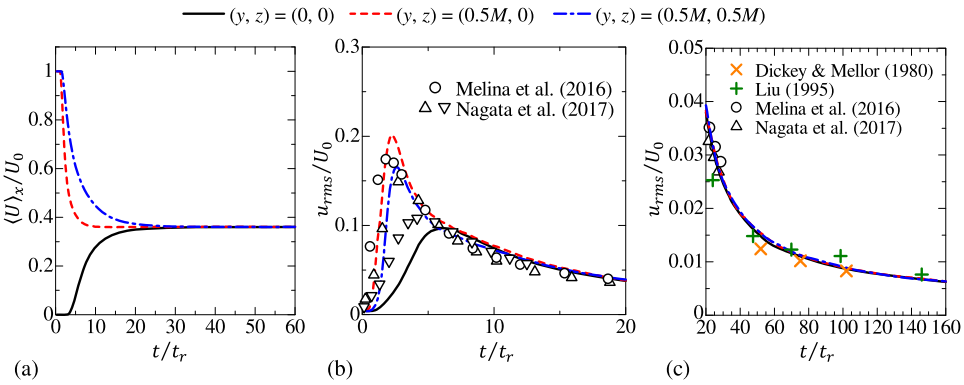

FIG. 7. Temporal evolutions of (a) mean velocity and [(b) and (c)] rms streamwise velocity u_{rms} at three y–z locations at $Re_M = 20\,000$. The present DNS results are compared with u_{rms} measured near the grid in wind tunnel experiments.[56,57] (c) also includes the results from towed-grid experiments.[58,59] The streamwise distance x in wind tunnel experiments is converted to time as x/U_∞ (U_∞: the inlet velocity) for comparison.

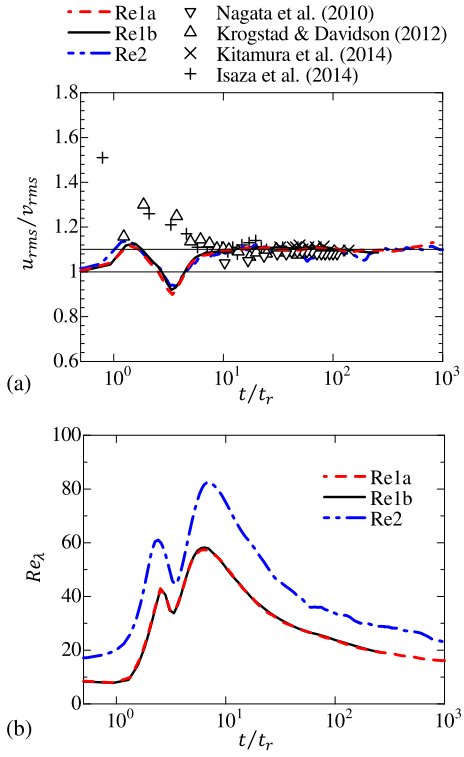

FIG. 8. Temporal evolution of (a) Reynolds stress ratios $u_{rms}/v_{rms} = \sqrt{\langle u'^2\rangle_x/\langle v'^2\rangle_x}$ compared with experiments and spatial DNS of the grid turbulence[13,18,19,22] and (b) Taylor Reynolds number $Re_\lambda = u_{rms}\lambda/\nu$ at $(y, z) = (0, 0)$. The thin solid lines in (a) indicate $u_{rms}/v_{rms} = 1.0$ and 1.1.

towed grid turbulence, which also decays in time rather than in space, is very close to the values obtained in our temporal simulations. The anisotropy of the temporally developing grid turbulence is examined using the ratio between the streamwise and transverse rms velocities $u_{rms}/v_{rms} = \sqrt{\langle u'^2\rangle_x/\langle v'^2\rangle_x}$. Figure 8(a) illustrates the temporal evolution of u_{rms}/v_{rms} at $(y, z) = (0, 0)$. The streamwise velocity fluctuations are higher than the transverse component ($u_{rms}/v_{rms} \approx 1.1$) for both Re_M values even after the turbulence is fully developed. The temporally developing grid turbulence is weakly anisotropic, in agreement with the wind tunnel experiments of grid turbulence, which have shown that u_{rms}/v_{rms} is larger than unity.[12–19] The level of anisotropy u_{rms}/v_{rms} in the present DNS is comparable with that in the experiments. Notably, u_{rms}/v_{rms} remains constant during decay, which is consistent with the experimental results of the spatially developing grid turbulence.[13,18,19] The difference can be found for the early time $t/t_r \le 4$ between the DNS and experiment. u_{rms}/v_{rms} has been hardly studied in the very near field behind the hole region of the grid, where the turbulence is not developed. The strong dependence on the grid geometry in the near field can cause the observed difference for the early time $t/t_r \le 4$.

Figure 8(b) shows the temporal evolution of the Taylor Reynolds number $Re_\lambda = u_{rms}\lambda/\nu$, where $\lambda = u_{rms}/\langle(\partial u'/\partial x)^2\rangle_x^{1/2}$ is calculated with the streamwise velocity. Re_λ has two peaks. The first one appears at $t/t_r \approx 2$. At this time, the grid turbulence is not fully developed, as shown in Fig. 3(b). The recent experiment involving the near field of the grid turbulence also shows a large value of Re_λ just behind the hole of the grid,[57] although the peak value and its location depend on the conditions. Re_λ reaches a maximum value at $t/t_r = 7$ and then begins to decay. For the decay period, $Re_\lambda = 58 - 15$ at $Re_M = 10\,000$ and $Re_\lambda = 82 - 22$ at $Re_M = 20\,000$. This Re_λ range is consistent with those in the grid turbulence experiments at similar Re_M.[17,18]

Figure 9 shows the ratio $(E_{uu}/E_{vv})^{1/2}$ between one-dimensional energy spectra of streamwise velocity and transverse velocity fluctuations. In large scales, the streamwise velocity fluctuation has a larger energy than the transverse velocity. The ratio $(E_{uu}/E_{vv})^{1/2}$ decreases with the wavenumber k_x and falls below 1, and the transverse velocity has higher energy in small scales. The DNS study of the spatially developing grid turbulence[26] shows the ratio of the one-dimensional energy spectrum of streamwise velocity and transverse velocity fluctuations, defined with the Fourier transform in the transverse direction. Their DNS also showed that the transverse velocity has a higher energy in small scale than the streamwise velocity fluctuation although it is opposite in large scales.

The skewness of the streamwise velocity derivative $\partial u'/\partial x$, defined as

$$S_{\partial u/\partial x} = \frac{\langle(\partial u'/\partial x)^3\rangle_x}{\langle(\partial u'/\partial x)^2\rangle_x^{3/2}}, \tag{9}$$

in the decay period of the grid turbulence, for which Re_λ decreases with time, is plotted against Re_λ in Fig. 10(a) along with comparisons against the grid turbulence experiments. We selected experimental data from previous studies so that the statistics can be compared at a similar level of Re_λ.

A wide range of the value is found to be obtained for $S_{\partial u/\partial x}$ in the grid turbulence for $20 < R_\lambda < 50$. Although $S_{\partial u/\partial x}$ approaches a universal constant for large Re_λ ($Re_\lambda \ge 70$), the way this constant is approached is flow-dependent.[62] The variation of $S_{\partial u/\partial x}$ for $20 < R_\lambda < 50$ in the grid turbulence might be attributed to a different grid geometry used in the experiments (e.g., solidity, square bar or rod), which is also different between the temporal and spatial simulations

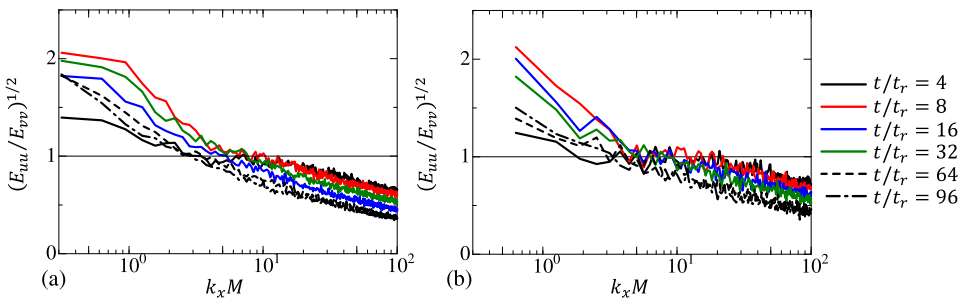

FIG. 9. Ratio between one-dimensional energy spectra of streamwise velocity and cross-streamwise velocity, $(E_{uu}/E_{vv})^{1/2}$, at $(y, z) = (0, 0)$ for (a) $Re_M = 10\,000$ and (b) $Re_M = 20\,000$, where E_{uu} and E_{vv} are computed with Fourier transform in the x direction.

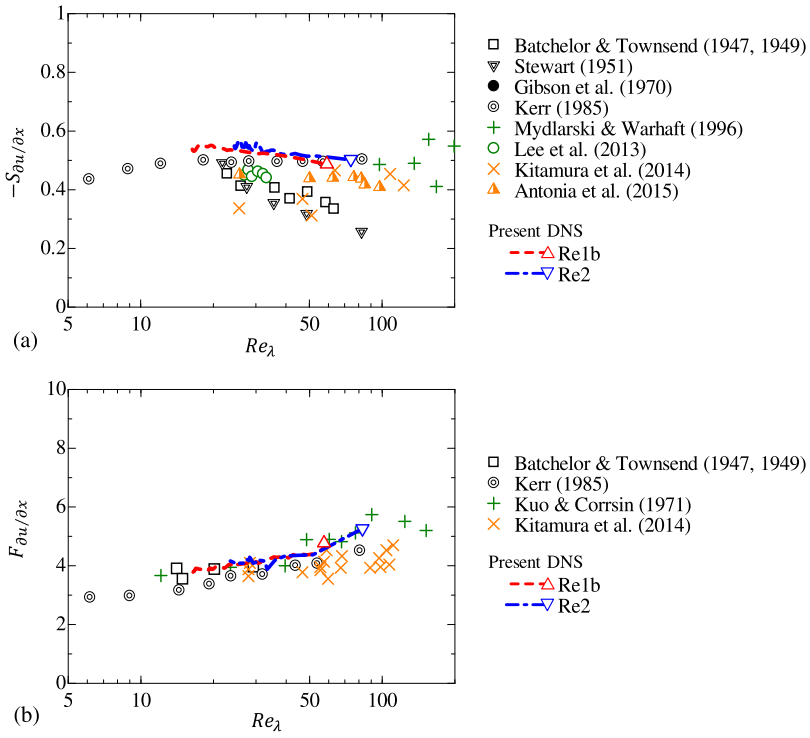

FIG. 10. (a) Skewness and (b) flatness of the streamwise velocity derivative plotted against Re_λ. The present DNS results are shown for time after Re_λ reaches the maximum values, which are marked by the symbols in the figures. The figures include the results of the experiments of grid turbulence[16,18,62–66] and circular jets[65] and numerical simulations of homogeneous isotropic turbulence.[67] Some of these results were compiled by Sreenivasan and Antonia.[68]

of the grid turbulence. $S_{\partial u/\partial x}$ in the present DNS is generally well within the variation observed in the previous experiments. Figure 10(b) shows the flatness of $\partial u'/\partial x$, defined as

$$F_{\partial u/\partial x} = \frac{\langle(\partial u'/\partial x)^4\rangle_x}{\langle(\partial u'/\partial x)^2\rangle_x^2}, \tag{10}$$

against Re_λ. The Re_λ-dependence is recovered well in the present DNS, which is consistent with the previous experiments and DNS.

Figure 11 depicts the temporal evolution of the normalized TKE dissipation rate $C_\varepsilon = \varepsilon L_u/u_{rms}^3$, where C_ε is calculated from the statistics at $(y, z) = (0, 0)$. C_ε is constant in the strictly homogeneous turbulence at a high Reynolds number. Indeed, C_ε at $Re_M = 20\,000$ in the present DNS hardly changes with time for $30 < t/t_r < 600$, for which the grid turbulence has almost reached a statistically homogeneous state, as can be seen in Figs. 5 and 6. C_ε increases with time at $Re_M = 10\,000$ because C_ε becomes large as Re_λ decreases for low Re_λ, which decays with time.

Note that the constant value of C_ε for $Re_M = 20\,000$ is larger than that in the forced homogeneous isotropic turbulence. This difference is explained by a spectral disequilibrium introduced by the influence of the nonlinear cascade time in the decaying turbulence.[69] Figure 11(b) shows that C_ε at $Re_M = 10\,000$ is close to constant only for the early stage of decay, which could be in an initial transient decay region.[20] For later time, Re_λ becomes so small that C_ε is no longer constant. Therefore, the behavior of the grid turbulence, such as the evolution of C_ε, is different between two Re_M. C_ε increases with time for $t/t_r \leq 30$ for both Re_M before the time independence of C_ε is achieved. A similar tendency is found in the grid turbulence experiments, where C_ε increases in the

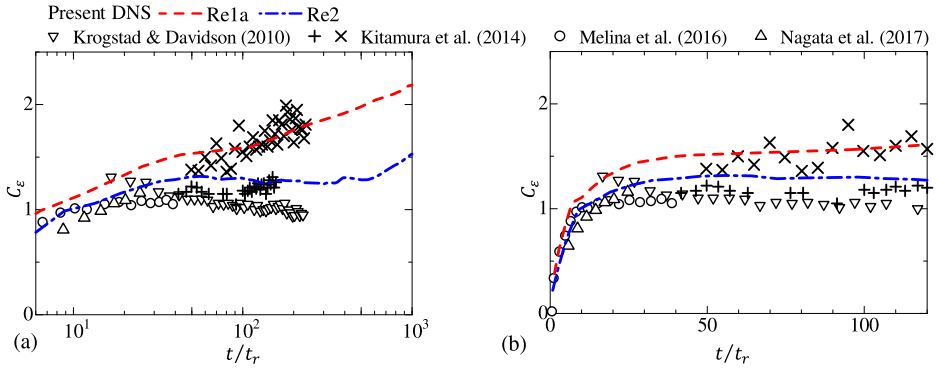

FIG. 11. Temporal evolution of C_ε at $(y, z) = (0, 0)$ in a (a) semi-logarithmic and (b) linear plot. The present DNS results are compared with C_ε measured in wind tunnel experiments of grid turbulence.[18,20,56,57] In these previous studies, Re_λ ranges between 90 and 70 in the work of Krogstad and Davidson,[20] 29 and 27 for × symbols and 50 and 47 for + symbols in the work of Kitamura *et al.*,[18] 239 and 63 in the work of Melina *et al.*,[56] and 267 and 76 in the work of Nagata *et al.*[57] Note that the results from the work of Melina *et al.*[56] and Nagata *et al.*[57] include the region just behind the grid, where Re_λ is very different from the decay region.

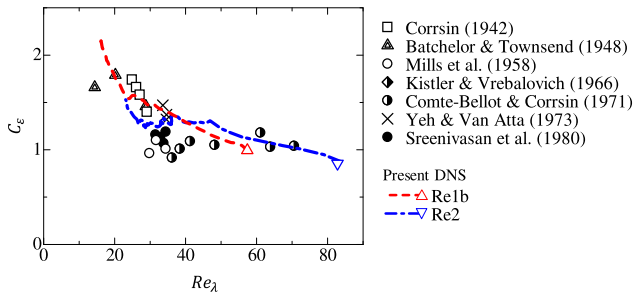

FIG. 12. C_ε is plotted against Re_λ, where the present DNS results are shown for the time after Re_λ reaches the maximum values marked by the symbols in the figure. The figure includes the grid turbulence data[12,24,75–79] compiled by Sreenivasan.[74]

streamwise direction near the grid before C_ε reaches a constant value.[56,57,70,71] This region with an increasing C_ε is often called the non-equilibrium region in grid turbulence.[70,72,73]

Figure 12 shows a plot of C_ε against Re_λ with the previous experimental data compiled by Sreenivasan.[74] Note that our results in Fig. 12(b) are presented for the time after Re_λ reaches a maximum value (i.e., decay period). The present results agree with the previous experiments. Furthermore, the increase in C_ε for the later time at $Re_M = 20\,000$ is caused by the low Reynolds number effect.[69] Therefore, C_ϵ at low Re_λ for $Re_M = 20\,000$ tends to merge with the curve obtained for $Re_M = 10\,000$. In the non-equilibrium region of grid turbulence, C_ϵ increases as Re_λ decays,[72] where C_ϵ also depends on Re_M. Therefore, at the early stage of decay, C_ϵ is different between $Re_M = 10\,000$ and 20 000 even for similar values of Re_λ.

The results presented above have shown that the statistics are very similar between the spatially and temporally developing grid turbulence. However, large-scale flow structures near the grid, which can be better described by two-point statistics, can be different because the flow characteristics significantly change in the streamwise direction near the grid. Nonetheless, it is remarkable that the turbulence produced from the simple initial mean velocity profile evolves in a very similar way as grid turbulence.

C. Decay of the grid turbulence

We investigate the decay law of the temporally developing grid turbulence. Accordingly, the power laws for the TKE decay are examined for the region with a constant C_ε at $Re_M = 20\,000$, whilst the time dependence of C_ε is considered at $Re_M = 10\,000$. The parameters in the following decay laws for $\langle u'^2\rangle_x$, which is equivalent to Eq. (4), are determined through a nonlinear least-squares method (i.e., the Levenberg–Marquardt method) applied to time $t_s \le t \le t_e$:

$$\frac{\langle u'^2\rangle_x}{U_0^2} = a\left(\frac{t}{t_r} - \frac{t_0}{t_r}\right)^{-n}, \tag{11}$$

where t_0 is the virtual origin and a is the decay constant. The decay exponent n is overestimated when a fitting includes the initial transient decay region.[20] Therefore, we exclude the initial transient decay period from the fitting, where this period can be identified by applying a least-squares method with reducing t_s because a larger value of the decay exponent is obtained when t_s is in the initial decay period. Furthermore, t_s is determined at $Re_M = 10\,000$ such that the time period with a constant C_ε is excluded in a fitting procedure because n needs to be corrected for considering the time dependence of C_ε. Because the DNS of Re1b is performed only until $t/t_r = 256$, the time period that is adequate for assessing the decay exponent is too short for both time-dependent and constant C_ε. Therefore, the decay exponent is studied with Re1a and Re2. For the same reason, the decay exponent at $Re_M = 20\,000$ is estimated from the time period with a constant C_ε. We apply fitting to the decay of $\langle u'^2\rangle_x$ for different sets of (t_s, t_e) under these conditions. Figure 13 presents the decay exponent n obtained in this manner. The decay exponent for $Re_M = 10\,000$ hardly changes with the fitting time period when (t_s, t_e) is chosen from the time period over which C_ε increases. We also find that $n \approx 1.2$ is obtained for $Re_M = 20\,000$ when the early time, $t_s \le 50$, is not included in the fitting. A large value of n obtained for $t_s \le 50$ is related to the transient regime of the decay. Note that we also obtain a large n for the same reason when the time period with constant C_ε for $Re_M = 10\,000$ was used for fitting [i.e., $n = 1.5$ for $(t_s/t_r, t_e/t_r) = (40, 120)$]. Hereafter, we use the results obtained by the fitting of Eq. (11) to time $(t_s, t_e) = (200t_r, 900t_r)$ at $Re_M = 10\,000$ and to $(t_s, t_e) = (100t_r, 500t_r)$ at $Re_M = 20\,000$. Table II summarizes the values of n, a, and t_0 of Eq. (11) and the rms error between the DNS data points and Eq. (11). The decay exponent at $Re_M = 20\,000$ is $n = 1.22$, which is fairly close to the value obtained for the Saffman turbulence. This n value is also close to that reported in the wind tunnel experiments of the grid turbulence.[18,20,80] The Saffman turbulence decays with the modified decay exponent[20] when C_ε follows a power law $C_\varepsilon = C(t/t_r - t_0/t_r)^p$ (C is a constant),

$$\langle u'^2\rangle_x \sim \left(\frac{t}{t_r} - \frac{t_0}{t_r}\right)^{-6(1+p)/5}. \tag{12}$$

Figure 14 shows the relation $C_\varepsilon = C(t/t_r - t_0/t_r)^p$ at $Re_M = 10\,000$, where a non-linear least-squares method yields $p = 0.13$. The present p value is close to the experimental

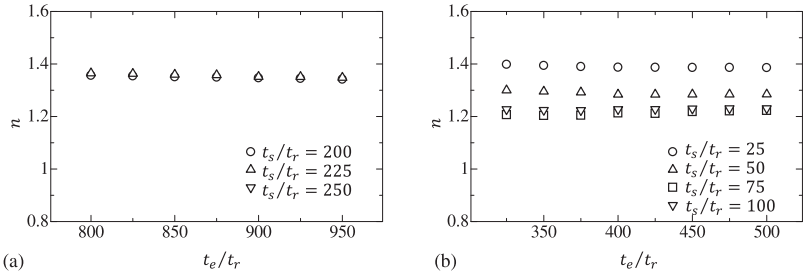

FIG. 13. Decay exponents obtained for different fitting times (t_s, t_e) at (a) $Re_M = 10\,000$ and (b) $Re_M = 20\,000$.

TABLE II. The parameters, n, a, and t_0, of the decay law [Eq. (11)] determined by a nonlinear least-squares method (the Levenberg-Marquardt method). E_r is the rms error between the DNS data points and Eq. (11) with the values of a, t_0, and n shown in the table.

Run	Re_M	n	a	t_0	E_r
Re1a	10 000	1.35	0.033	$2.7t_r$	2.0×10^{-8}
Re2	20 000	1.22	0.016	$18t_r$	4.0×10^{-7}

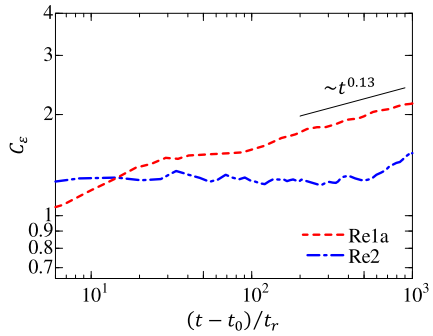

FIG. 14. Logarithmic plot of C_ε against $t - t_0$ at $(y, z) = (0, 0)$. The virtual origin t_0 is the same as in Table II.

value ($p \simeq 0.1$) of the grid turbulence at a low Reynolds number.[18] The decay exponent of TKE expected for the Saffman turbulence is then $6(1 + p)/5 \approx 1.36$ at $Re_M = 10\,000$, which agrees well with the estimated value of $n = 1.35$ obtained using a least-squares method to $\langle u'^2 \rangle_x$.

The evolutions of L_u, ε, and λ for the Saffman turbulence with a constant C_ε are written as follows:[20]

$$L_u \sim \left(\frac{t}{t_r} - \frac{t_0}{t_r}\right)^{\frac{2}{5}}, \quad \varepsilon \sim \left(\frac{t}{t_r} - \frac{t_0}{t_r}\right)^{-\frac{11}{5}}, \quad \frac{\lambda}{M} = \left[\frac{25}{3Re_M}\left(\frac{t}{t_r} - \frac{t_0}{t_r}\right)\right]^{\frac{1}{2}}. \tag{13}$$

We obtain the following relations for the Saffman turbulence with $C_\varepsilon = C(t/t_r - t_0/t_r)^p$:[20]

$$L_u \sim \left(\frac{t}{t_r} - \frac{t_0}{t_r}\right)^{\frac{2(1+p)}{5}}, \quad \varepsilon \sim \left(\frac{t}{t_r} - \frac{t_0}{t_r}\right)^{-\frac{(11+6p)}{5}}, \quad \frac{\lambda}{M} = \left[\frac{25(1+p)^{-1}}{3Re_M}\left(\frac{t}{t_r} - \frac{t_0}{t_r}\right)\right]^{\frac{1}{2}}. \tag{14}$$

The temporal evolutions of L_u, λ, and ε in the DNS are compared with the equations in Figs. 15 and 16. The DNS results agree well with the power laws for the Saffman turbulence with both cases of constant and time-dependent C_ε. Kitamura *et al.*[18] also found that dependence of C_ε on small Re_λ causes a non-zero positive value of p in grid turbulence at a low Reynolds number, where L_u and λ were found to obey Eq. (14) instead of Eq. (13). Their experimental results for a higher Reynolds number confirmed Eq. (13) similarly to our DNS at $Re_M = 20\,000$.

D. Three-dimensional energy spectrum and Saffman integral

The statistics presented in Subsection III C well follow the scaling laws obtained for the Saffman turbulence. This result implies that $E(k)$ for low wavenumbers is approximated by the first term with the Saffman integral in Eq. (1). The Saffman integral is computed in the grid turbulence from Eq. (2), whose integral is computed over $0 \le |\mathbf{r}| \le r_0$, where r_0 is the first separation distance at which $\langle \mathbf{u}(\mathbf{x}) \cdot \mathbf{u}(\mathbf{x} + r_0 \mathbf{e}_x) \rangle$ reaches 0 ($\mathbf{e}_x$: unit vector in the x direction). Figure 17(a) shows the temporal evolutions of L for $t/t_r \ge 32$ in all simulations. L decays until $t \approx 200t_r$ while it tends to be constant for $t \ge 200t_r$. The decay of L before $t \approx 200t_r$ follows the power law $L/U_0^2 M^3 = a(t/t_r)^b$. The least squares method applied to $0 \le t/t_r \le 200$ yields $(a, b) = (6.02 \times 10^{-4}, -0.281)$ for Re1a,

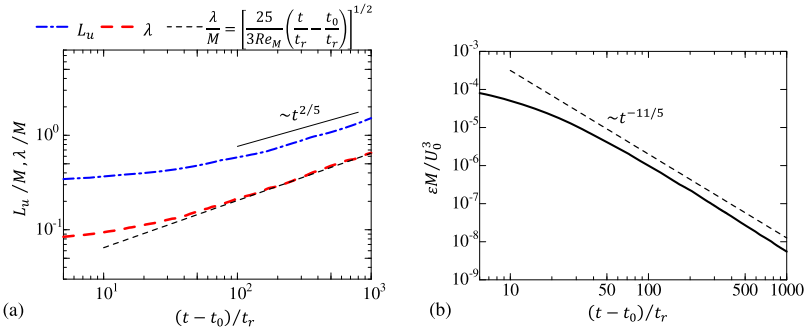

FIG. 15. (a) Temporal evolutions of integral length scale L_u and Taylor microscale λ. (b) Decay of the TKE dissipation rate. The results are shown at $Re_M = 20\,000$. The figures also show the power laws for these quantities in the Saffman turbulence with a constant C_ε.

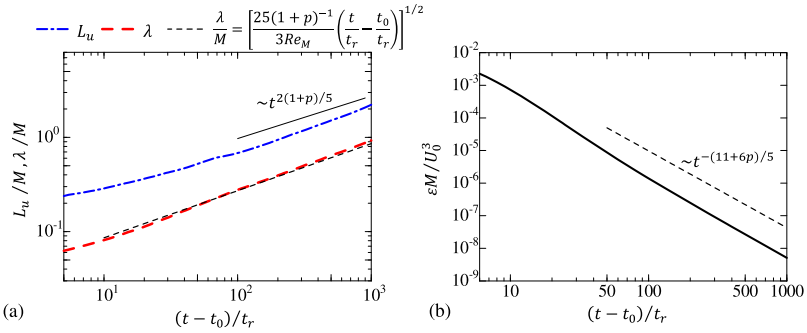

FIG. 16. The same as in Fig. 15 but at $Re_M = 10\,000$. The figures also show the power laws for the Saffman turbulence with $C_\varepsilon = C(t/t_r - t_0/t_r)^p$.

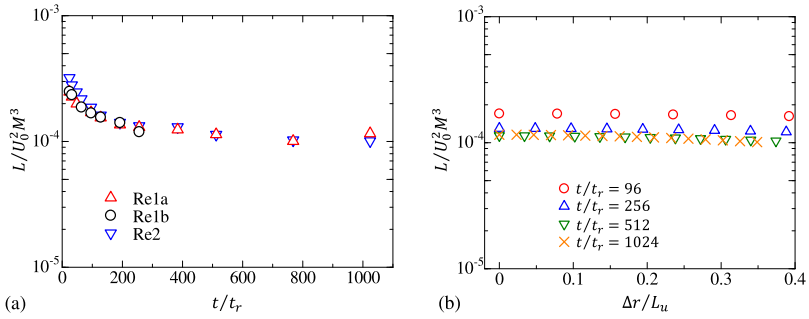

FIG. 17. (a) Temporal evolutions of L obtained from Eq. (2), where the integral is computed over $0 \le |\mathbf{r}| \le r_0$ with r_0 defined as $\langle \mathbf{u}(\mathbf{x}) \cdot \mathbf{u}(\mathbf{x} + r_0\mathbf{e}_x) \rangle = 0$. (b) L computed with the integral over $0 \le |\mathbf{r}| \le r_0 - \Delta r$ plotted against Δr in Re1a.

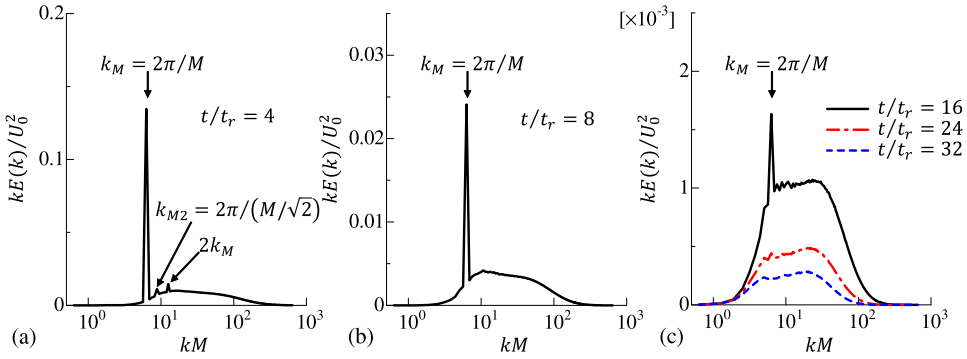

FIG. 18. Three-dimensional energy spectra $E(k)$ at $Re = 20\,000$ in an area-preserving form at (a) $t/t_r = 4$, (b) $t/t_r = 8$, and (c) $t/t_r = 16$, 24, and 32. The wavenumber of peaks is shown in the figures.

$(a, b) = (6.13 \times 10^{-4}, -0.282)$ for Re1b, and $(a, b) = (1.12 \times 10^{-3}, -0.395)$ for Re2.

The influence of the domain used for the integral in Eq. (2) is investigated in Fig. 17(b), where the integral in Eq. (2) is taken for $0 \le |\mathbf{r}| \le r_0 - \Delta r$. The decrease in L with Δr is very small, and small changes in r_0 hardly affect L estimated by Eq. (2). The power laws confirmed for the statistics indicate that the grid turbulence simulated in this study is close to the Saffman type, for which the first term in Eq. (1), that is to say L, is not negligible. Figure 17 also shows that L does not diminish as zero and is conserved during decay for $t \ge 200t_r$.

A three-dimensional energy spectrum $E(k)$ is computed from $\mathbf{u}$. Figure 18 shows the temporal development of $E(k)$

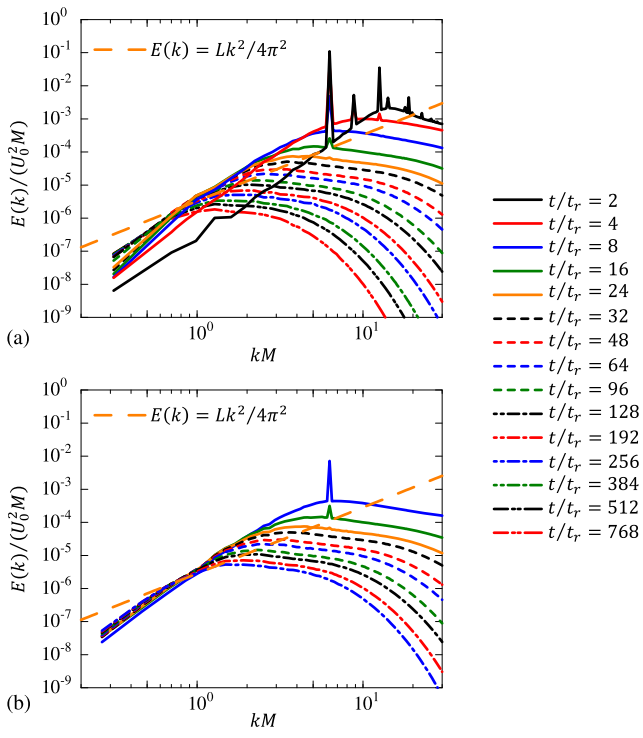

FIG. 19. Three-dimensional energy spectra $E(k)$ at $Re_M = 10\,000$ of (a) Re1a and (b) Re1b. $E(k)$ is compared with $Lk^2/4\pi^2$, where L is taken at $t = 256t_r$.

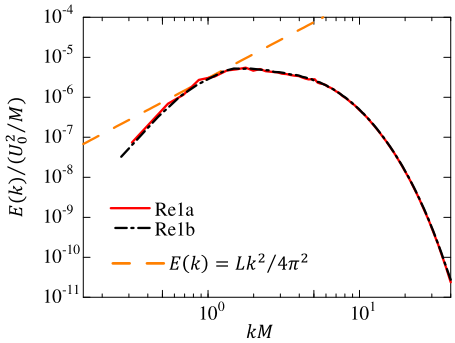

FIG. 20. Comparison of $E(k)$ at $Re_M = 10\,000$ between Re1a and Re1b at $t = 256t_r$ with $E(k) = Lk^2/4\pi^2$ for Re1b.

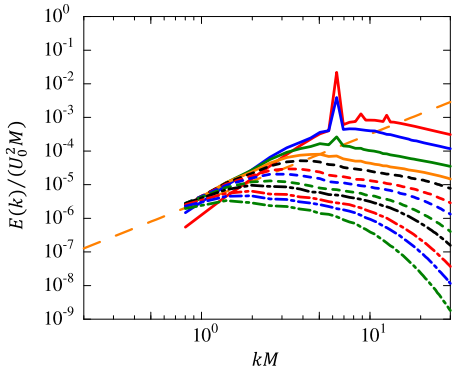

FIG. 21. Three-dimensional energy spectra $E(k)$ at $Re_M = 20\,000$, where L is taken at $t = 256t_r$. The lines are the same as in Fig. 19.

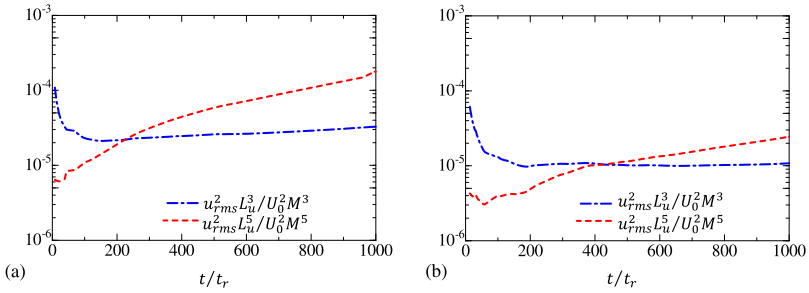

FIG. 22. Temporal evolutions of $u_{rms}^2 L_u^3$ and $u_{rms}^2 L_u^5$ at $(y, z) = (0, 0)$ at (a) $Re_M = 10\,000$ and (b) $Re_M = 20\,000$.

at the initial stage of the simulation. The peaks in $E(k)$ found for $t/t_r = 4$, 8, and 16 are related to the geometry of the turbulence grid considered: the wavenumbers of the mesh size $k_M = 2\pi/M$ and the diagonal length of the mesh $k_{M2} = 2\pi/\sqrt{2}M$. $E(k)$ computed for Eq. (8) also exhibits large peaks at these wavenumbers. These peaks disappear once the mean velocity profile becomes homogeneous at $t/t_r = 24$.

Figure 19 shows $E(k)$ at $Re_M = 10\,000$ in comparison with the first term of Eq. (1), where L is computed with Eq. (2) at $t = 256t_r$. $E(k)$ has large peaks at the wavenumber related to the grid geometry. As these peaks decay, $E(k)$ at lower wavenumbers increases with time. In later time, although $E(k) \approx Lk^2/4\pi$ is not valid in the limit of $k \to 0$ unlike in the theoretical framework of the Saffman turbulence, there is a wavenumber range for which $E(k) \approx Lk^2/4\pi$ holds in the temporally developing grid turbulence: $E(k) \approx Lk^2/4\pi$ is valid for $0.8 \le kM \le 1.3$, which corresponds to $0.1 \le k/k_L \le 0.2$, where $k_L = 2\pi/L_u$. These are the length scales about 5-10 times larger than the integral length scale. Figure 20 compares $E(k)$ at $Re_M = 10\,000$ between Re1a and Re1b at $t = 256t_r$. Even though the simulations of Re1a and Re1b are performed with different domain sizes, they result in a very similar shape of $E(k)$, and the wavenumber range with $E(k) \approx Lk^2/4\pi$ is not different for Re1a and Re1b. Figure 21 shows $E(k)$ at $Re_M = 20\,000$. Although the computational domain is small in this case, $E(k)$ at a low wavenumber increases with time, and a wavenumber range for which $E(k) \approx Lk^2/4\pi$ gradually appears with time. $E(k)$ at $Re_M = 10\,000$ is not approximated by $E(k) \approx Lk^2/4\pi$ for $kM \le 0.8$, and the spectral shape is inconsistent with the theory. These wavenumbers of $kM \le 0.8$ are not expressed by the present DNS at $Re_M = 20\,000$ because of the computational domain size. However, temporal evolutions of various statistics confirm that the temporally developing grid turbulence behaves like the Saffman turbulence. One might consider that the departure from $E(k) \approx Lk^2/4\pi$ for $kM \le 0.8$ at $Re_M = 10\,000$ is due to the influence of the computational domain size. However, both Re1a and Re1b observe the departure from $E(k) \approx Lk^2/4\pi$ for a similar wavenumber range in Fig. 20, and Re2 with the smallest computational domain does not clearly show $E(k) < Lk^2/4\pi$ even though the computational domain is smaller in Re2 than Re1a and Re1b. These results show that $E(k) < Lk^2/4\pi$ for $kM \le 0.8$ is not caused by an insufficient domain size. Even when the wavenumber range $kM \le 0.8$ does not exist in the flow (Re2), and even when $E(k)$ does not follow $Lk^2/4\pi$ for $kM \le 0.8$ (Re1a and Re1b), the temporally developing grid turbulence decays according to the Saffman decay law. It is indicated that the decay of grid turbulence is not affected by the spectral shape of $kM \le 0.8$. We can roughly estimate the smallest wavenumber that can be expressed in the present simulation as the wavenumber of the side length of the domain l, defined as $k_l = 2\pi/l$. In wind-tunnel experiments of grid turbulence, the smallest wavenumber is related to the length of the cross section of wind tunnels, L_{WT}, where the corresponding wavenumber is $k_{WT} = 2\pi/L_{WT}$. Here, L_{WT} is the length of the short side when the test section has a rectangular shape. In experiments of grid turbulence by Kitamura *et al.*,[18] $k_{WT}M$ has a value between $0.13 \le k_{WT}M \le 0.7$. Krogstad and Davidson[20] used the wind tunnel and grid that gave $k_{WT}M = 0.14$. The experiments by Sinhuber *et al.*[21] had $k_{WT}M = 0.75$. Because of different shapes of wind tunnels, the influence of the wall on $E(k)$ for $k \approx k_{WT}$ must be very different among these experiments. However, all of these experiments have observed the decay of grid turbulence that follows the Saffman decay law even though $E(k)$ for $k \approx k_{WT}$ must be influenced by the wall. Our DNS and previous experiments of grid turbulence imply that the wavenumber range of $0.8 \lesssim kM$ has only a negligible influence on the decay of grid turbulence.

The conservation of the linear momentum in a fully developed Saffman turbulence requires that $u_{rms}^2 L_u^3$ is constant. Meanwhile, the conservation of the angular momentum for the Batchelor turbulence demands $u_{rms}^2 L_u^5$ to be constant. These invariants are used to assess whether the grid turbulence follows the Saffman or the Batchelor type in the experiments.[18,20] Figure 22 shows the temporal evolution of $u_{rms}^2 L_u^3$ and $u_{rms}^2 L_u^5$. $u_{rms}^2 L_u^5$ increases with time, whilst $u_{rms}^2 L_u^3$ is close to constant in later time as expected for the Saffman turbulence. These behaviors of $u_{rms}^2 L_u^5$ and $u_{rms}^2 L_u^3$ agree with the grid turbulence experiments.[18,20] The time dependence of $u_{rms}^2 L_u^3$ is expected from Fig. 17. $u_{rms}^2 L_u^3$ rapidly decreases at the early time of the simulations during which the turbulence is produced for $t/t_r \le 32$. Furthermore, $u_{rms}^2 L_u^3$ around $t/t_r = 100$ is still decreasing with time in Fig. 22, for which the Saffman integral L also decays in Fig. 17. The decrease in $u_{rms}^2 L_u^3$ in the initial decay region also agrees with the experiments.[18,20]

IV. CONCLUSIONS

We have performed direct numerical simulations of a temporally developing grid turbulence, which is a counterpart of the spatially developing grid turbulence widely studied in experiments and direct numerical simulations. This temporal approach is inspired by the temporal simulations of free shear flows, including turbulent wakes, because the grid turbulence is generated from the wakes of many grid bars. The temporal grid turbulence is statistically homogeneous in the streamwise direction while the actual grid turbulence is not,

especially in the near field of the grid, where the turbulence is produced. The present study is limited to this temporal model of grid turbulence, and the influences of inhomogeneity in the streamwise direction might have an influence on the large-scale characteristics. Nevertheless, the comparisons between the temporally and spatially developing grid turbulences have shown that these two flows are very similar in terms of the evolutions of various statistics both in the production and decay regions.

Extensive discussions of whether the grid turbulence is of a Saffman or Batchelor type or neither have long existed. This argument has been based on the decay exponent n of TKE or $\langle u^2 \rangle L_u^{m+1}$, where $m = 2$ for the Saffman turbulence and $m = 4$ for the Batchelor turbulence. Previous studies have not clarified how the nature of the Saffman or Batchelor turbulence prevails in the production region before grid turbulence begins to decay. This issue requires us to investigate the temporal evolution of a three-dimensional energy spectrum $E(k)$ in both production and decay regions of grid turbulence because the large scale properties of grid turbulence in the decay region are expected to be determined in the production region, where $E(k)$ at a low wavenumber also evolves with time from the initial laminar state. The temporal approach enables us to simulate the grid turbulence in a periodic box. We have directly calculated the three-dimensional energy spectrum $E(k)$ and Saffman integral L based on the present DNS of the grid turbulence at mesh Reynolds numbers of $Re_M = 10\,000$ and $20\,000$ with a large periodic box compared with the mesh size M (thus, integral length scale L_u). The Taylor Reynolds number Re_λ during decay ranges from 58 to 15 for $Re_M = 10\,000$ and from 82 to 22 at $Re_M = 20\,000$.

The decay exponent n of the variance of the streamwise velocity fluctuation is $n = 1.22$ at $Re_M = 20\,000$ and $n = 1.35$ at $Re_M = 10\,000$, which are close to the values for the Saffman turbulence 6/5 for $Re_M = 20\,000$ and $6(1 + p)/5 \approx 1.36$ for $Re_M = 10\,000$, where $p \approx 0.13$ is obtained from $C_\varepsilon \sim t^p$ at large t. The evolutions of the longitudinal integral scale, Taylor microscale, and the TKE dissipation rate are also consistent with the Saffman turbulence. The Saffman integral tends to be time-independent after the turbulence evolves for about $200M/U_0$. A direct evaluation of the TKE spectrum $E(k)$ shows that $E(k) \approx Lk^2/4\pi^2$ is valid for a finite range of low wavenumbers that correspond to length scales of 5-10 times of the integral length scale. However, the limiting behavior of $E(k \to 0)$ does not follow $E(k \to 0) \sim k^2$, which is assumed in the theoretical framework of the Saffman turbulence. Nevertheless, the temporal evolutions of the turbulence statistics agree well with the theoretical prediction based on the Saffman turbulence, which can be related to $E(k) \approx Lk^2/4\pi^2$ in a low but finite wavenumber range.

The temporally developing grid turbulence is generated from a mean streamwise velocity profile that approximates the flow past a grid. This approximation ignores various possible influences of grid geometry and can be appropriate only for the mean streamwise profile. However, the turbulence generated in this way has many common features with grid turbulence studied in experiments. Furthermore, it decays in consistent with the Saffman decay law. These results imply that the mean streamwise velocity profile formed by a flow past a grid has very important roles in the formation of grid turbulence that follows the Saffman decay law.

ACKNOWLEDGMENTS

The numerical simulations were carried out on the high-performance computing system (NEC SX-ACE) in the Japan Agency for Marine-Earth Science and Technology. This work was supported by JSPS KAKENHI Grant Nos. 18H01367 and 18K13682 and partially by the "Collaborative Research Project on Computer Science with High-Performance Computing in Nagoya University."

[1] R. O. Fox, *Computational Models for Turbulent Reacting Flows* (Cambridge University Press, 2003).
[2] D. Veynante and L. Vervisch, "Turbulent combustion modeling," Prog. Energy Combust. Sci. **28**, 193–266 (2002).
[3] G. L. Mellor and T. Yamada, "Development of a turbulence closure model for geophysical fluid problems," Rev. Geophys. **20**, 851–875, https://doi.org/10.1029/rg020i004p00851 (1982).
[4] A. J. Arnfield, "Two decades of urban climate research: A review of turbulence, exchanges of energy and water, and the urban heat island," Int. J. Climatol. **23**, 1–26 (2003).
[5] G. K. Batchelor, *The Theory of Homogeneous Turbulence* (Cambridge University Press, 1953).
[6] P. A. Davidson, *Turbulence: An Introduction for Scientists and Engineers* (Oxford University Press, 2004).
[7] P. G. Saffman, "The large-scale structure of homogeneous turbulence," J. Fluid Mech. **27**, 581–593 (1967).
[8] G. K. Batchelor and I. Proudman, "The large-scale structure of homogeneous turbulence," Philos. Trans. R. Soc., A **248**, 369–405 (1956).
[9] A. N. Kolmogorov, "On the degeneration of isotropic turbulence in an incompressible viscous fluid," Dokl. Akad. Nauk SSSR **31**, 319–323 (1941).
[10] S. B. Pope, *Turbulent Flows* (Cambridge University Press, 2000).
[11] L. F. G. Simmons and C. Salter, "Experimental investigation and analysis of the velocity variations in turbulent flow," Proc. R. Soc. A **145**, 212–234 (1934).
[12] G. Comte-Bellot and S. Corrsin, "The use of a contraction to improve the isotropy of grid-generated turbulence," J. Fluid Mech. **25**, 657–682 (1966).
[13] K. Nagata, H. Suzuki, Y. Sakai, and T. Hayase, "Direct numerical simulation of turbulence with scalar transfer around complex geometries using the immersed boundary method and fully conservative higher-order finite-difference schemes," in *Numerical Simulations, Applications, Examples and Theory* (INTECH, 2010).
[14] H. L. Grant and I. C. T. Nisbet, "The inhomogeneity of grid turbulence," J. Fluid Mech. **2**, 263–272 (1957).
[15] M. S. Uberoi and S. Wallis, "Effect of grid geometry on turbulence decay," Phys. Fluids **10**, 1216–1224 (1967).
[16] L. Mydlarski and Z. Warhaft, "On the onset of high-Reynolds-number grid-generated wind tunnel turbulence," J. Fluid Mech. **320**, 331–368 (1996).
[17] P. Lavoie, L. Djenidi, and R. A. Antonia, "Effects of initial conditions in decaying turbulence generated by passive grids," J. Fluid Mech. **585**, 395–420 (2007).
[18] T. Kitamura, K. Nagata, Y. Sakai, A. Sasoh, O. Terashima, H. Saito, and T. Harasaki, "On invariants in grid turbulence at moderate Reynolds numbers," J. Fluid Mech. **738**, 378–406 (2014).
[19] J. C. Isaza, R. Salazar, and Z. Warhaft, "On grid-generated turbulence in the near- and far field regions," J. Fluid Mech. **753**, 402–426 (2014).
[20] P.-Å. Krogstad and P. A. Davidson, "Is grid turbulence Saffman turbulence?," J. Fluid Mech. **642**, 373–394 (2010).
[21] M. Sinhuber, E. Bodenschatz, and G. P. Bewley, "Decay of turbulence at high Reynolds numbers," Phys. Rev. Lett. **114**, 034501 (2015).
[22] P.-Å. Krogstad and P. A. Davidson, "Near-field investigation of turbulence produced by multi-scale grids," Phys. Fluids **24**, 035103 (2012).
[23] L. Djenidi, M. Kamruzzaman, and R. A. Antonia, "Power-law exponent in the transition period of decay in grid turbulence," J. Fluid Mech. **779**, 544–555 (2015).
[24] G. K. Batchelor and A. A. Townsend, "Decay of isotropic turbulence in the initial period," Proc. R. Soc. A **193**, 539–558 (1948).

[25]K. Nagata and S. Komori, "The difference in turbulent diffusion between active and passive scalars in stable thermal stratification," J. Fluid Mech. **430**, 361–380 (2001).
[26]K. Nagata, H. Suzuki, Y. Sakai, T. Hayase, and T. Kubo, "Direct numerical simulation of turbulence characteristics generated by fractal grids," Int. Rev. Phys **2**, 400–409 (2008).
[27]S. Laizet and J. C. Vassilicos, "DNS of fractal-generated turbulence," Flow, Turbul. Combust. **87**, 673–705 (2011).
[28]S. Laizet and J. C. Vassilicos, "Stirring and scalar transfer by grid-generated turbulence in the presence of a mean scalar gradient," J. Fluid Mech. **764**, 52–75 (2015).
[29]Y. Zhou, K. Nagata, Y. Sakai, H. Suzuki, Y. Ito, O. Terashima, and T. Hayase, "Relevance of turbulence behind the single square grid to turbulence generated by regular- and multiscale-grids," Phys. Fluids **26**, 075105 (2014).
[30]C. B. da Silva and J. C. F. Pereira, "Invariants of the velocity-gradient, rate-of-strain, and rate-of-rotation tensors across the turbulent/nonturbulent interface in jets," Phys. Fluids **20**, 055101 (2008).
[31]M. van Reeuwijk and M. Holzner, "The turbulence boundary of a temporal jet," J. Fluid Mech. **739**, 254–275 (2014).
[32]P. J. Diamessis, G. R. Spedding, and J. A. Domaradzki, "Similarity scaling and vorticity structure in high-Reynolds-number stably stratified turbulent wakes," J. Fluid Mech. **671**, 52–95 (2011).
[33]J. Philip, I. Bermejo-Moreno, D. Chung, and I. Marusic, "Characteristics of the entrainment velocity in a developing wake," in International Symposium on Turbulence and Shear Flow Phenomena (TSFP-9), 30 June–3 July 2015, Melbourne Australia, available online at http://www.tsfp-conference.org/proceedings/2015/v3/9C-5.pdf.
[34]M. Gampert, J. Boschung, F. Hennig, M. Gauding, and N. Peters, "The vorticity versus the scalar criterion for the detection of the turbulent/non-turbulent interface," J. Fluid Mech. **750**, 578–596 (2014).
[35]W. D. Smyth and J. N. Moum, "Length scales of turbulence in stably stratified mixing layers," Phys. Fluids **12**, 1327–1342 (2000).
[36]M. Kozul, D. Chung, and J. P. Monty, "Direct numerical simulation of the incompressible temporally developing turbulent boundary layer," J. Fluid Mech. **796**, 437–472 (2016).
[37]T. Watanabe, X. Zhang, and K. Nagata, "Turbulent/non-turbulent interfaces detected in DNS of incompressible turbulent boundary layers," Phys. Fluids **30**, 035102 (2018).
[38]X. Zhang, T. Watanabe, and K. Nagata, "Turbulent/non-turbulent interfaces in high-resolution direct numerical simulation of temporally evolving compressible turbulent boundary layers," Phys. Rev. Fluids **3**, 094605 (2018).
[39]S. Laizet, J. Nedić, and J. C. Vassilicos, "Influence of the spatial resolution on fine-scale features in DNS of turbulence generated by a single square grid," Int. J. Comput. Fluid Dyn. **29**, 286–302 (2015).
[40]L. Skrbec and S. R. Stalp, "On the decay of homogeneous isotropic turbulence," Phys. Fluids **12**, 1997–2019 (2000).
[41]M. Meldi, P. Sagaut, and D. Lucor, "A stochastic view of isotropic turbulence decay," J. Fluid Mech. **668**, 351–362 (2011).
[42]M. Meldi and P. Sagaut, "Further insights into self-similarity and self-preservation in freely decaying isotropic turbulence," J. Turbul. **14**, 24–53 (2013).
[43]X. Wu, "Inflow turbulence generation methods," Annu. Rev. Fluid. Mech. **49**, 23–49 (2017).
[44]R. D. Moser, M. M. Rogers, and D. W. Ewing, "Self-similarity of time-evolving plane wakes," J. Fluid Mech. **367**, 255–289 (1998).
[45]J. P. Hickey, F. Hussain, and X. Wu, "Role of coherent structures in multiple self-similar states of turbulent planar wakes," J. Fluid Mech. **731**, 312–363 (2013).
[46]J. P. Hickey, F. Hussain, and X. Wu, "Compressibility effects on the structural evolution of transitional high-speed planar wakes," J. Fluid Mech. **796**, 5–39 (2016).
[47]A. G. Kravchenko and P. Moin, "Numerical studies of flow over a circular cylinder at $Re_D = 3900$," Phys. Fluids **12**, 403–417 (2000).
[48]J. G. Wissink and W. Rodi, "Numerical study of the near wake of a circular cylinder," Int. J. Heat Fluid Flow **29**, 1060–1070 (2008).
[49]A. Kempf, M. Klein, and J. Janicka, "Efficient generation of initial-and inflow-conditions for transient turbulent flows in arbitrary geometries," Flow, Turbul. Combust. **74**, 67–84 (2005).
[50]R. E. Seoud and J. C. Vassilicos, "Dissipation and decay of fractal-generated turbulence," Phys. Fluids **19**, 105108 (2007).
[51]Y. Morinishi, T. S. Lund, O. V. Vasilyev, and P. Moin, "Fully conservative higher order finite difference schemes for incompressible flow," J. Comput. Phys. **143**, 90–124 (1998).
[52]H. A. Van der Vorst, "Bi-CGSTAB: A fast and smoothly converging variant of Bi-CG for the solution of nonsymmetric linear systems," SIAM J. Sci. Stat. Comput. **13**, 631–644 (1992).
[53]T. Watanabe and K. Nagata, "Mixing model with multi-particle interactions for Lagrangian simulations of turbulent mixing," Phys. Fluids **28**, 085103 (2016).
[54]T. Watanabe, C. B. da Silva, and K. Nagata, "Multi-particle dispersion during entrainment in turbulent free-shear flows," J. Fluid Mech. **805**, R1 (2016).
[55]T. Watanabe, J. J. Riley, K. Nagata, R. Onishi, and K. Matsuda, "A localized turbulent mixing layer in a uniformly stratified environment," J. Fluid Mech. **849**, 245–276 (2018).
[56]G. Melina, P. J. K. Bruce, and J. C. Vassilicos, "Vortex shedding effects in grid-generated turbulence," Phys. Rev. Fluids **1**, 044402 (2016).
[57]K. Nagata, T. Saiki, Y. Sakai, Y. Ito, and K. Iwano, "Effects of grid geometry on non-equilibrium dissipation in grid turbulence," Phys. Fluids **29**, 015102 (2017).
[58]T. D. Dickey and G. L. Mellor, "Decaying turbulence in neutral and stratified fluids," J. Fluid Mech. **99**, 13–31 (1980).
[59]H.-T. Liu, "Energetics of grid turbulence in a stably stratified fluid," J. Fluid Mech. **296**, 127–157 (1995).
[60]T. Michioka and S. Komori, "Large-eddy simulation of a turbulent reacting liquid flow," AIChE J. **50**, 2705–2720 (2004).
[61]O. Praud, A. M. Fincham, and J. Sommeria, "Decaying grid turbulence in a strongly stratified fluid," J. Fluid Mech. **522**, 1–33 (2005).
[62]R. A. Antonia, S. L. Tang, L. Djenidi, and L. Danaila, "Boundedness of the velocity derivative skewness in various turbulent flows," J. Fluid Mech. **781**, 727–744 (2015).
[63]G. K. Batchelor and A. A. Townsend, "Decay of vorticity in isotropic turbulence," Proc. R. Soc. A **190**, 534–550 (1947).
[64]G. K. Batchelor and A. A. Townsend, "The nature of turbulent motion at large wave-numbers," Proc. R. Soc. A **199**, 238–255 (1949).
[65]A. Y.-S. Kuo and S. Corrsin, "Experiments on internal intermittency and fine-structure distribution functions in fully turbulent fluid," J. Fluid Mech. **50**, 285–319 (1971).
[66]S. K. Lee, L. Djenidi, R. A. Antonia, and L. Danaila, "On the destruction coefficients for slightly heated decaying grid turbulence," Int. J. Heat Fluid Flow **43**, 129–136 (2013).
[67]R. M. Kerr, "Higher-order derivative correlations and the alignment of small-scale structures in isotropic numerical turbulence," J. Fluid Mech. **153**, 31–58 (1985).
[68]K. R. Sreenivasan and R. A. Antonia, "The phenomenology of small-scale turbulence," Annu. Rev. Fluid. Mech. **29**, 435–472 (1997).
[69]W. J. T. Bos, L. Shao, and J.-P. Bertoglio, "Spectral imbalance and the normalized dissipation rate of turbulence," Phys. Fluids **19**, 045101 (2007).
[70]P. C. Valente and J. C. Vassilicos, "Universal dissipation scaling for nonequilibrium turbulence," Phys. Rev. Lett. **108**, 214503 (2012).
[71]J. Hearst and P. Lavoie, "Decay of turbulence generated by a square-fractal-element grid," J. Fluid Mech. **741**, 567–584 (2014).
[72]J. C. Vassilicos, "Dissipation in turbulent flows," Annu. Rev. Fluid. Mech. **47**, 95–114 (2015).
[73]P. C. Valente and J. C. Vassilicos, "The decay of turbulence generated by a class of multiscale grids," J. Fluid Mech. **687**, 300–340 (2011).
[74]K. R. Sreenivasan, "On the scaling of the turbulence energy dissipation rate," Phys. Fluids **27**, 1048–1051 (1984).
[75]S. Corrsin, "Decay of turbulence behind three similar grids," A. E. thesis, CIT, 1942.
[76]R. R. Mills, A. L. Kistler, V. O'brien, and S. Corrsin, "Turbulence and temperature fluctuations behind a heated grid," NACA Technical Notes 4288, 1958.
[77]A. L. Kistler and T. Vrebalovich, "Grid turbulence at large Reynolds numbers," J. Fluid Mech. **26**, 37–47 (1966).
[78]T. T. Yeh and C. W. Van Atta, "Spectral transfer of scalar and velocity fields in heated-grid turbulence," J. Fluid Mech. **58**, 233–261 (1973).
[79]K. R. Sreenivasan, S. Tavoularis, R. Henry, and S. Corrsin, "Temperature fluctuations and scales in grid-generated turbulence," J. Fluid Mech. **100**, 597–621 (1980).
[80]J. Hearst and P. Lavoie, "Effects of multi-scale and regular grid geometries on decaying turbulence," J. Fluid Mech. **803**, 528–555 (2016).